International Forum on Aeroelasticity and Structural Dynamics
IFASD 2024
17-21 June 2024, The Hague, The Netherlands

EXPERIMENTAL INVESTIGATION OF A HIGHLY FLEXIBLE WING

Giuliano Coppotelli[1], Roberto Giovanni Sbarra[1], Ludovica Onofri[1], Marcello Righi[2]

[1]Università "La Sapienza"
Department of Mechanical and Aerospace Engineering
Via Eudossiana, 18 184, Roma, Italy
giuliano.coppotelli@uniroma1.it

[2]School of Engineering
Zurich University of Applied Sciences
8401 Winterthur, Switzerland
rigm@zhaw.ch

Keywords: Structural dynamics, Aeroelasticity, Operational Modal Analysis, Wind Tunnel Testing

Abstract: This study focuses on the experimental characterization of the dynamic response of a high aspect ratio flexible wind tunnel model (PAZY wing). Numerous studies have shown that flutter appears as a hump mode, influenced by the static aeroelastic solution, which in turn affects the coupling of the second bending and first torsional modes. By installing the same model in different wind tunnels and modifying the boundary conditions, this study emphasizes the significance of even the smallest details in such analyses. Furthermore, it demonstrates the effectiveness of Operational Modal Analysis (OMA) based approaches. Lastly, the study sheds light on the subcritical nature of the Limit Cycle Oscillations (LCO) exhibited at three, five, and seven degrees of incidence at the wing root. It reveals that the system's response as it approaches the flutter onset speed depends on the strength of external perturbations, which can drive the system toward either the trivial solution or the LCO.

NOMENCLATURE

BR	=	Balanced Realization
CFD	=	Computational Fluid Dynamics
FDD	=	Frequency Domain Decomposition
FRF	=	Frequency Response Function
HTM	=	Hilbert Transform Method
LCO	=	Limit Cycle Oscillations
OMA	=	Operational Modal Analysis
PSD	=	Power Spectral Densities
$RANS$	=	Reynolds Averaged Nvier Stokes equations
SSI	=	Stochastic Subspace Identification

1 INTRODUCTION

Flexible aircraft structures have gained popularity due to higher aerodynamic efficiency and lighter design concepts. The aeroelasticity of these systems involves nonlinear static aeroelastic

solutions and complex behaviors at the linear stability boundary, including Limit Cycle Oscillations (LCO) and sub-critical unstable solutions. The Third Aeroelastic Prediction Workshop (January 2023) focused on the stability analysis of such structures, particularly examining the "PAZY wing" model proposed by Daniella Raveh of Technion.

Aeroelastic Prediction Workshops, held regularly since 2011, assess the accuracy of numerical techniques in capturing structural and aerodynamic nonlinearities. Details of past workshops can be found on their respective websites ([1–3] and in several referenced studies [4–11].

The PAZY wing, by design, exhibits large static bending displacements under aerodynamic loads. Simple wind tunnel experiments reveal several flutter mechanisms, primarily a "handbook" bending-torsion flutter involving the second bending and first torsional modes. The mode coupling depends heavily on static bending deflection and dynamic pressure, resulting in flutter appearing as a hump mode. Experimental investigations at Technion (refer to [12, 13]) provided a reference flutter boundary for numerical analysis and showed that instability develops into LCO. Numerous studies have since been published on this topic [12, 14–29].

Most researchers used low-order models, combining finite element beam models with linear 2D or 3D aerodynamics, for instance in Refs. [14, 17, 30]. Aerodynamic forces were modelled using conventional approaches like strip theory, vortex-lattice methods, doublet-lattice methods, and panel methods. These studies generally agreed well with experimental data, as summarized in Ritter's paper in Ref. [31].

Additional experiments by various teams have expanded the understanding of the PAZY wing [12, 13, 26, 29, 32, 33]. Preliminary findings from one experimental campaign, involving the same model in two different wind tunnels, were published by the authors [29]. One unresolved issue from the Third Aeroelastic Prediction Workshop was the subcritical nature of LCO and its amplitude dependence on wind speed. Riso provided further insights in a recent study [30].

This study aims to provide a new and more accurate experimental characterization of LCO. Data from two experimental campaigns have been post-processed, offering insights into the linear stability boundary and nonlinear behavior of the model. Measurements confirm that flutter is triggered by the coupling of the second bending and first torsional modes, consistent with existing studies. The data also supports the hypothesis of subcritical instability for certain angles of attack.

A unique feature of this study is the installation of two nearly identical PAZY wing models in two distinctly different wind tunnels: one at Rome "La Sapienza" and the other at the Zurich University of Applied Sciences. Additional testing was individually conducted by the authors at the University of Southampton (first author) and the Federal Institute of Technology in Zurich (fourth author), although these tests are not documented here.

Another distinctive aspect of this work is the use of Operational Modal Analysis (OMA) to characterize the dynamic response of the model. OMA methods rely on the hypothesis of broadband excitation loading, such as white noise, within the frequency range of interest. These methods utilize both time and frequency domain data. Modal parameters are estimated from the Power Spectral Density matrix using Frequency Domain Decomposition or the Hilbert Transform methods [34, 35], or through correlation functions as proposed in Stochastic Subspace Identification-based methods [36].

In this study, OMA methods were applied to the response accelerations recorded during wind tunnel tests to estimate natural frequencies, damping ratios, and mode shapes at different test points, corresponding to various combinations of wind tunnel velocity and wing model angle of attack. Since OMA methods provide accurate identification of these modal parameters, they allow for the assessment of the capability of different OMA methods to track the evolution of such parameters under varying operational conditions.

This article is structured as follows: section 2 presented methodologies and experimental facilities, section 3 presents and discusses results and section 4 the conclusions.

2 METHODOLOGIES AND EXPERIMENTAL FACILITIES

2.1 Design and Manufacturing of Wind Tunnel Models

2.1.1 Geometry and Materials

The PAZY wing is a straight, non-tapered wing with an aspect ratio of 11, designed not only to exhibit large deflections but also to be easily built with a few, simple tools and a 3D printer. The load-carrying part of the structure is an aluminum alloy spar with a length of 550 mm, a width of 60 mm, and a thickness of 2.5 mm. The external surface is composed of a thin Oralight foil and is secured by a number of 3D-printed webs. It is also possible to attach a 3D-printed slender cylindrical body (pencil) to the tip of the wing. Originally conceived as supporting elements for ballast, these attachments are known to alter the wing's torsional properties [37]. The wind tunnel models used in our studies are consistent with the original PAZY model proposed by Raveh. However, we built the models with a 2 mm thick spar instead of 2.5 mm. This choice was made to reduce flutter speed and make the experiments more suitable for our facilities. Additionally, the 2 mm aluminum alloy sheets were more readily available.

2.1.2 Instrumentation

Eight unidirectional accelerometers have been uniformly placed along the wing span, four on the leading edge and four on the trailing edge, to measure the vertical acceleration responses corresponding to the different airflow velocities. Those eight accelerometers are mounted internally on the aluminum spar to prevent aerodynamic interference. The time acquisitions are then collected through the *SIEMENS - Mobile Recorder*.

2.2 Operational Modal Analysis Methods (OMA)

The research team at the Structural Dynamics Laboratory of the Department of Mechanical and Aerospace Engineering at the University of Rome "La Sapienza" has developed a MATLAB routine known as NIMA [38]. This routine encompasses a variety of OMA methods, which permit the estimation of modal parameters in operational conditions. Among the aforementioned methods, there are FDD, HTM, and SSI (in time and frequency).

In the FDD algorithm, Power Spectral Densities (PSD) of response signals are computed and a Singular Value Decomposition (SVD) at each frequency lines available in the analysis is performed to estimate the natural frequencies and the mode shapes. Therefore, the damping ratios are evaluated from the corresponding single degree of freedom impulse response function evaluated in the neighborhood of the just identified natural frequencies. [39].

The HTM algorithm, on the other hand, estimates the biased Frequency Response Functions (FRFs), from which the modal parameters are estimated through least-squared curve fitting

employing a fractional function series expansion approximation. It's pertinent to note that the estimated FRFs are biased due to the absence of measured input excitation levels. Additionally, HTM handles closely spaced poles through SVD transformation [38].

The remaining two algorithms, Stochastic Subspace Identification (SSI) and Balanced Realization (BR), evaluate time responses. Both methods utilize correlation functions arranged in a Hankel matrix to construct a system matrix describing responses. The system matrix can be derived using various scaling methods to calculate an observability matrix containing a chosen number of influential singular values. Modal parameters are then extracted by solving the eigenvalue problem [39].

The air turbulence is capable of randomly exciting the Pazy wing model at each test point in the whole frequency range of the analysis. This random excitation, with white uncorrelated noise characteristics, allows to use of OMA, which is lastly performed through the use of the *NIMA* numerical procedure.

2.3 Wind Tunnel at "La Sapienza"

The experimental activity is carried out in the subsonic, closed circuit, and open test-section wind tunnel of the Mechanical and Aerospace Engineering Department at the University of Rome "La Sapienza", see Fig. 1. The circular test section has a diameter of 1 m and a length of 1.5 m, the free-stream velocity being variable between 5 and 40 m/s, with a background turbulent intensity equal to 0.3% at 15 m/s. The use of an open test section avoids the effect of growing boundary layers on the wind tunnel walls. The wind tunnel test section cross area is equal to about 0.75 m^2, with a solid blockage error due to the wing model volume evaluated as equal to less than 0.1%.

To have consistent structural boundary conditions with the wind tunnel at ZHAW, a rigid support is used to constrain the wing, as shown in Fig. 1. The stiffness of the attachment was measured and considered high enough not to interfere with the model's lowest modes, refer to Ref. [29] for additional details.

It is worthwhile mentioning that the effective and geometric angles of attack differ in wind tunnel experiments, depending on the type of test section and model size (with respect to the test section size). As such, the angle of attack values mentioned in this paper for one or the other infrastructure are not directly comparable. A qualitative conversion rule for the angle of attack in the two wind tunnels is proposed in section 3.2.

2.4 Wind Tunnel Testing at ZHAW

The Wind Tunnel ALFA at the Zurich University of Applied Sciences has a closed test section of 1.2 m length, 0.6 m height, and 0.9 m width. Wind speed in the test section can reach 50 m/s. The PAZY wing model was originally developed for a much bigger wind tunnel [33] and can only be installed in the ALFA wind tunnel by lowering the balance a few centimeters below the floor, as shown in Fig. 2. By doing so, the PAZY wing tip clears the wind tunnel ceiling only by a few centimeters. As such, we expect the tip vortex to be less effective and the PAZY wing to be aerodynamically more effective than in larger wind tunnels with a lower wind speed sufficient to reach flutter.

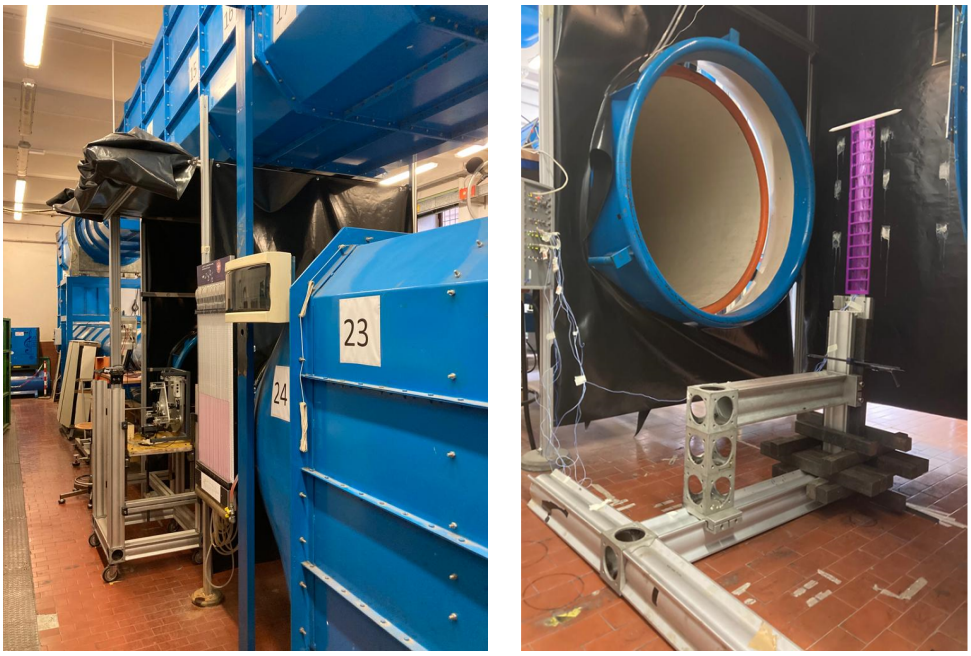

Figure 1: General view of the wind tunnel at “La Sapienza” and test layout.

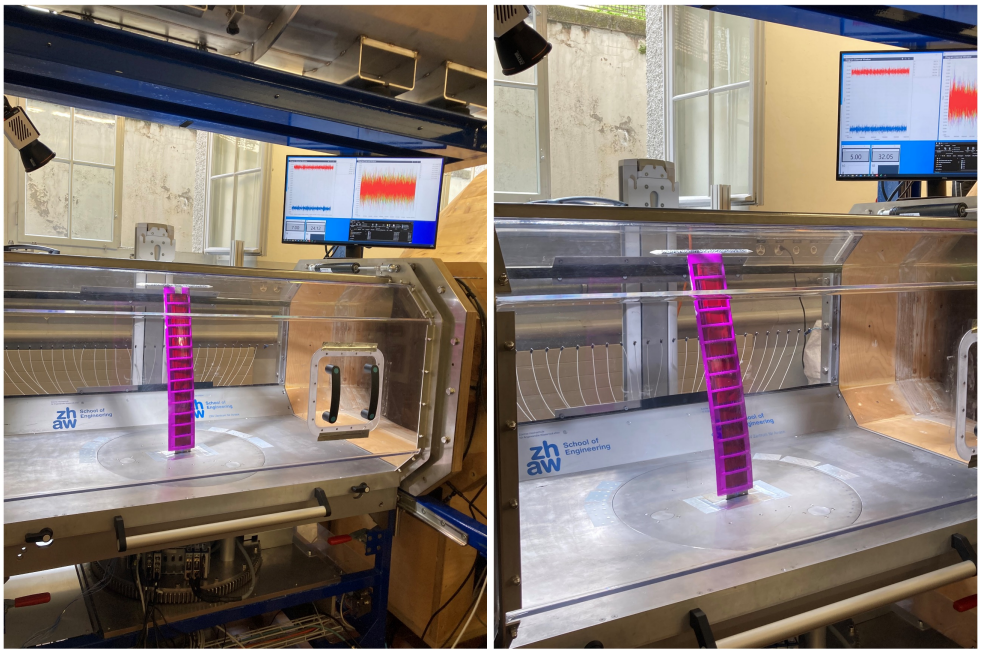

Figure 2: PAZY wing installed in the Wind Tunnel at ZHAW, under aerodynamic loading at low speed.

2.5 Analytical Model

The mathematical model used in this study was developed from analytical methods in aerodynamics and structural dynamics, and only fine-tuned with CFD data. A detailed description is provided in Ref. [26]. The model employs finite elements (conventional beam elements) for the structural components and strip theory for aerodynamics. Aerodynamic forces are evaluated at fifteen wing sections corresponding to the structural degrees of freedom. Additionally, a state-space aerodynamic model is generated following the methodology outlined by Leishman in Ref. [40], incorporating non-circulatory terms as detailed in Ref. [41]. The unsteady formulation adheres to Theodorsen’s theory [42].

The lift coefficient for each wing section is derived from a look-up table created from two-dimensional CFD simulations, which accurately capture the lift and drag forces generated by a NACA0018 airfoil at various Reynolds numbers. The lift curve slope is directly obtained from these simulations. The transitional SST (Langtry-Menter formulation, as in Ref. [43]) RANS turbulence model was used. CFD also captures the three-dimensionality of the flow in terms of the spanwise distribution of circulation, added separately as a correction term. All CFD calculations were conducted using the SU2 suite [44] with the compressible solver.

Large deflections are accounted for in the static aeroelastic solution by splitting the load into several smaller steps and iteratively rotating the stiffness matrix. Stability analysis is performed using the tangent mass and stiffness matrices, which are directly input into a state-space aeroelastic model.

The components and the flow of information are presented in the flowchart in Fig. 3.

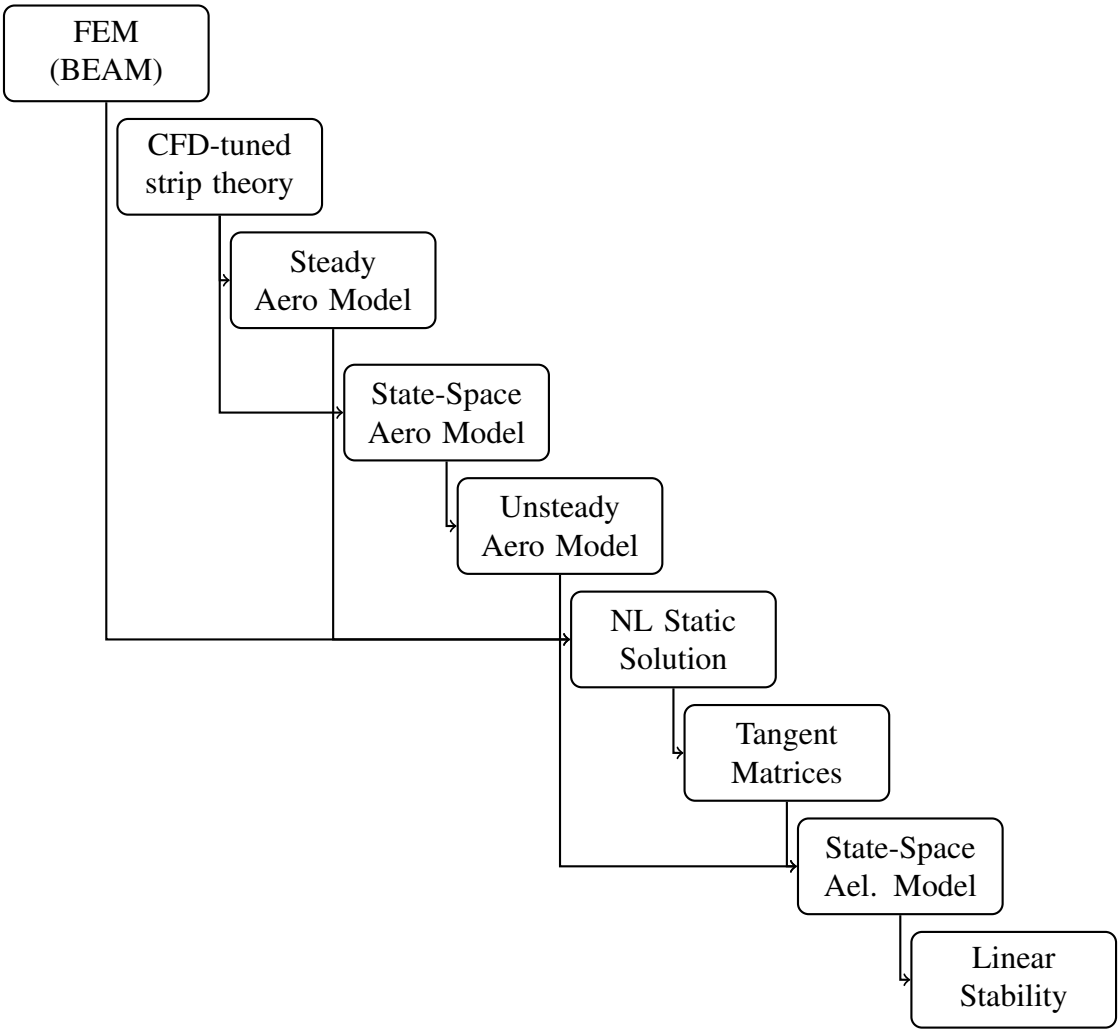

Figure 3: The flowchart shows the main components of the analytical model. The arrows represent the information flow between blocks.

Note that the model is kept simple by design. Tuning concerns the mass and the first five natural frequencies of the model. Regrettably, the influence of the wind tunnel's upper wall on the tip vortex is not yet taken into account.

3 RESULTS

3.1 Experiments carried out in the ZHAW wind tunnel

These experiments are the closest to the original PAZY investigations [12, 18] in that the wind tunnel has a closed test section and the model is clamped at the wind tunnel floor.

3.1.1 Linear stability analysis

Flutter onset and offset speeds are plotted in Figure 4 against the root angle of attack and compared to the predictions from the analytical model. The deviations are in the range of one to two m/s, and for almost all angles of attack, they fall within the uncertainties. However, the experimental values display a slightly different trend: both onset and offset speeds vary almost linearly with the angle of attack, whereas the predictions show much smaller changes with increasing root angle of attack, which aligns with most published results. We believe this is due to reduced aerodynamic efficiency in the 5-7 degree region and higher efficiency above 7 degrees. This may be attributed to the particular position of the wing tip near the wind tunnel's upper wall; furthermore, the upper wall has a small rectangular opening that was left open to allow rapid access to the model. The position of the opening is such that it might have affected the most the flow around the model precisely in the 5-7 degrees region. In practice, due to the effect of the aeroelastic static deflection of the model. the wing tip is placed closer to the opening for these angles of attack. This might have limited the aerodynamic effectiveness and requested a higher dynamic pressure to reach flutter. Note that no attempt other than tuning the natural frequencies and the mass was made to match predictions with experimental results.

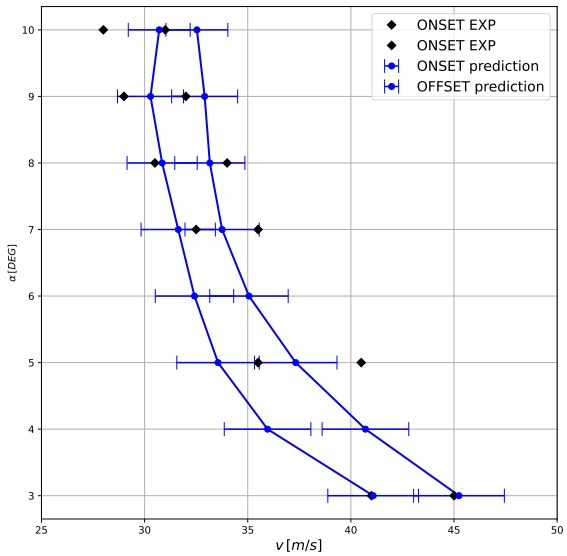

Figure 4: Flutter boundary.

Figures 5 and 7 present the experimental and analytical root locus captured at a three-degree root angle of attack. Figures 6 and 8 present the real (V-g plots) and the imaginary parts of the eigenvalues plotted against the wind speed. In all plots, the flutter mechanism is triggered by the coupling of the second bending and first torsional modes. Both the experimental results and the analytical predictions show that the first torsional eigenfrequency strongly decreases with increasing dynamic pressure. This is intuitive as the static elastic bending significantly increases the inertia associated with this mode, which is consistent with existing literature.

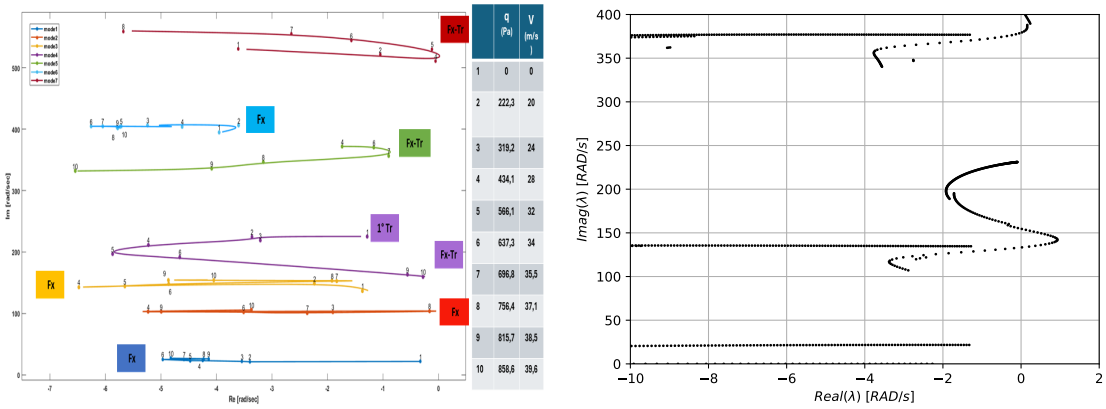

Figure 5: PAZY wing model: root locus at 3 degrees AoA.

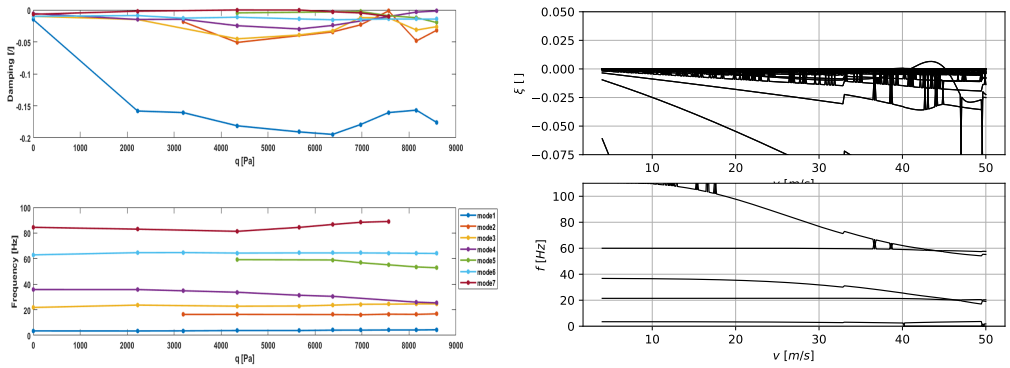

Figure 6: PAZY wing model: V-g plot at 3 degrees AoA.

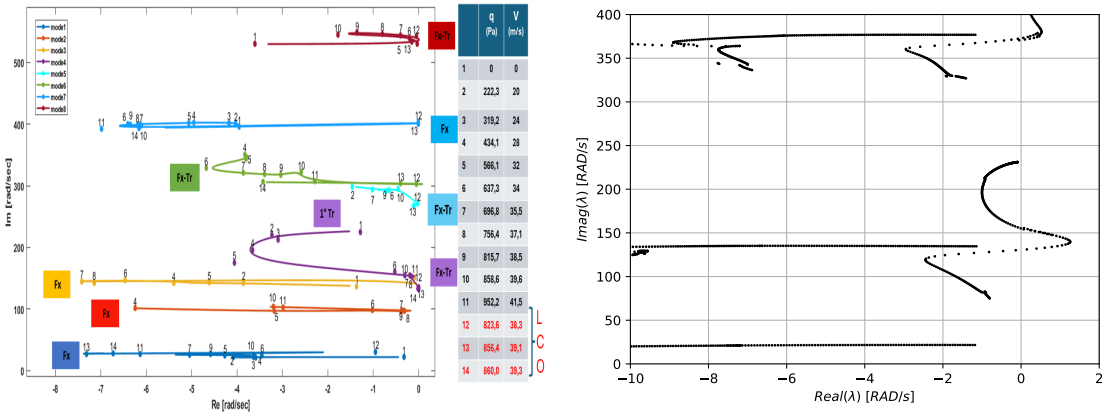

Figure 7: PAZY wing model: root locus at 5 degrees AoA.

It is important to note that the experiment reveals an additional mode, the second-lowest eigenfrequency, which is not visible in the predictions or in the literature. We suspect this mode is associated with the wind tunnel balance and does not influence the other modes or affect the flutter mechanism.

Furthermore, it is observed from both sources that even the second torsional and the third bending modes tend to coalesce at nearly the same dynamic pressure. Since this phenomenon is not documented in the literature, we hypothesize that it occurs due to the smaller spar thickness (2.0 mm instead of 2.5 mm).

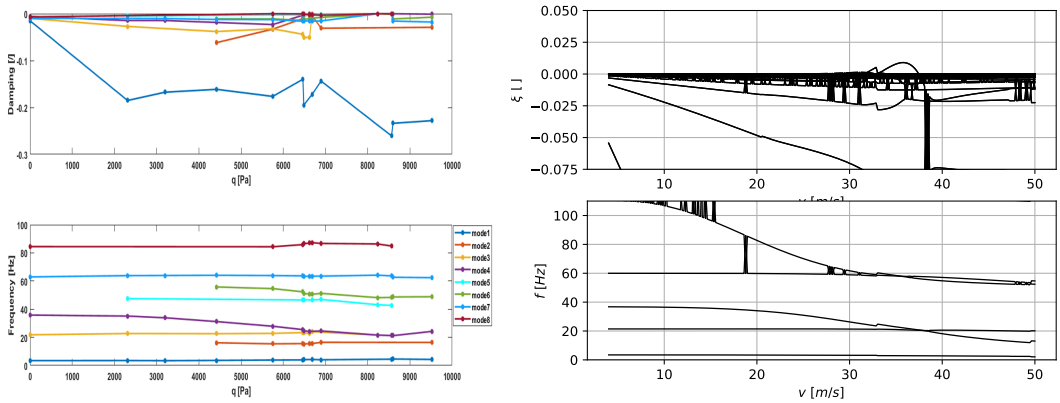

Figure 8: PAZY wing model: V-g plot at 5 degrees AoA.

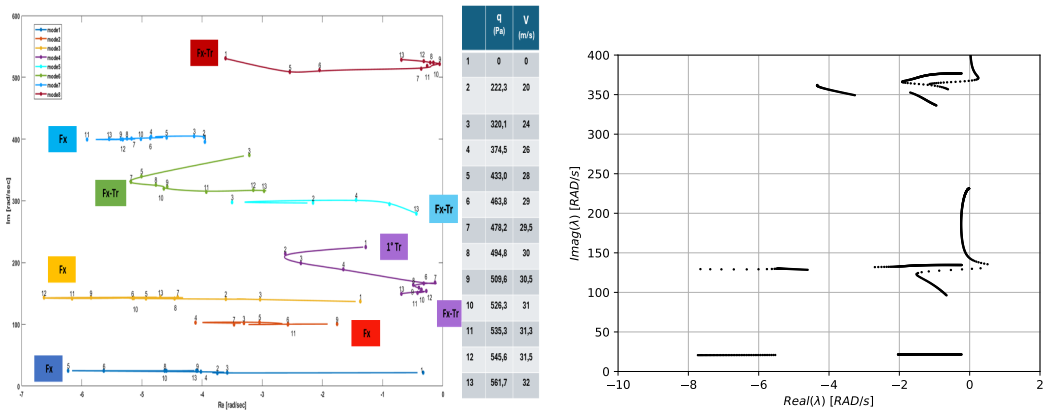

Figure 9: PAZY wing model: root locus at 7 degrees AoA.

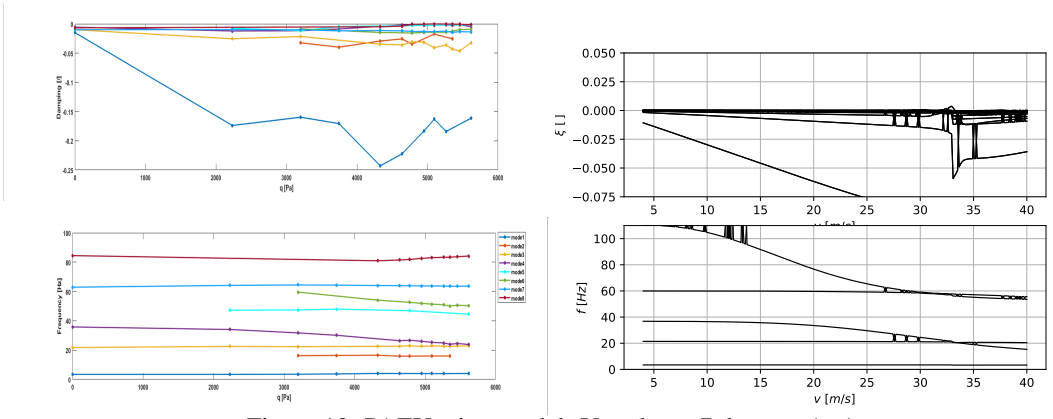

Figure 10: PAZY wing model: V-g plot at 7 degrees AoA.

Overall, the agreement between experiment and prediction is good; however, a large discrepancy is observed in the real part of the eigenvalues.

3.1.2 LCO analysis

Figure 11 summarizes the measurements taken within the unstable regime. For safety reasons, at all three root angles of attack, it was not possible to allow the model to oscillate freely for more than a few seconds, except in a few cases near the offset speed value at 5 and 7 degrees. Notably, the instability region at 3 degrees extended to the maximum capacity of the wind tunnel, and a complete offset could not be observed.

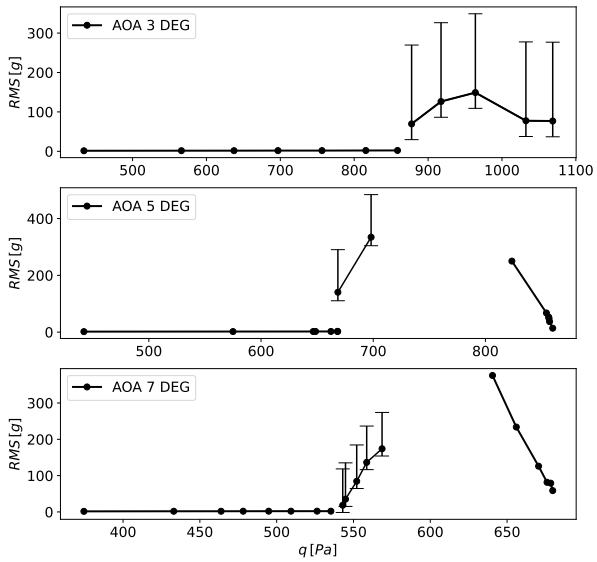

Figure 11: LCO Amplitude.

These observations suggest that the LCO appears (onset) abruptly and disappears (offset) more gradually. Furthermore, during dedicated investigations, by approaching the LCO onset very slowly, we identified a very narrow wind speed interval in which two or even three solutions could be observed. Specifically, a small external perturbation would be quickly damped out; larger perturbations would trigger the full LCO, and in some cases, intermediate amplitude perturbations would result in a different LCO with a much smaller amplitude, which would transition into the larger LCO within 20 to 30 seconds. This observation aligns perfectly with the iconic LCO image published by E.H. Dowell [45], which illustrates that a subcritical LCO branch can result in three possible solutions within a small speed interval. The intermediate solution is traditionally classified as an ”unstable LCO branch,”, which matches our observations, as this intermediate LCO tends to vanish after a short period. This behaviour is shown in Figures 12, 13, 14 and 15, which present the time signals from the 8 accelerometers.

LCO at angle of attack of 3 degrees. The response in time is shown in Figure 12. The wind tunnel turbulence is sufficient to trigger the flutter onset at this specific dynamic pressure. From the analysis of the signal, we notice that the system is unstable, develops rapidly increasing oscillations, and is stopped with an external intervention to avoid damage.

LCO at angle of attack of 5 degrees . The response in time is shown in Figure 13. The wind tunnel turbulence is not sufficient to trigger the flutter onset at this specific dynamic pressure. A smaller perturbation is introduced in correspondence with the green arrow and slowly evolves into rapidly increasing oscillations which must be interrupted with an external intervention to avoid damages.

LCO at angle of attack of 7 degrees (signal 1) . The time response shown in Figure 14 is obtained with a dynamic pressure chosen in correspondence of flutter onset. The wind tunnel turbulence is not sufficient to trigger the flutter onset at this specific dynamic pressure. Small perturbations are introduced in correspondence with the green arrows. The first one is not sufficient to immediately drive the system onto the stable LCO but makes an unstable LCO branch temporarily appear, the system subsequently evolves into the stable LCO. The second

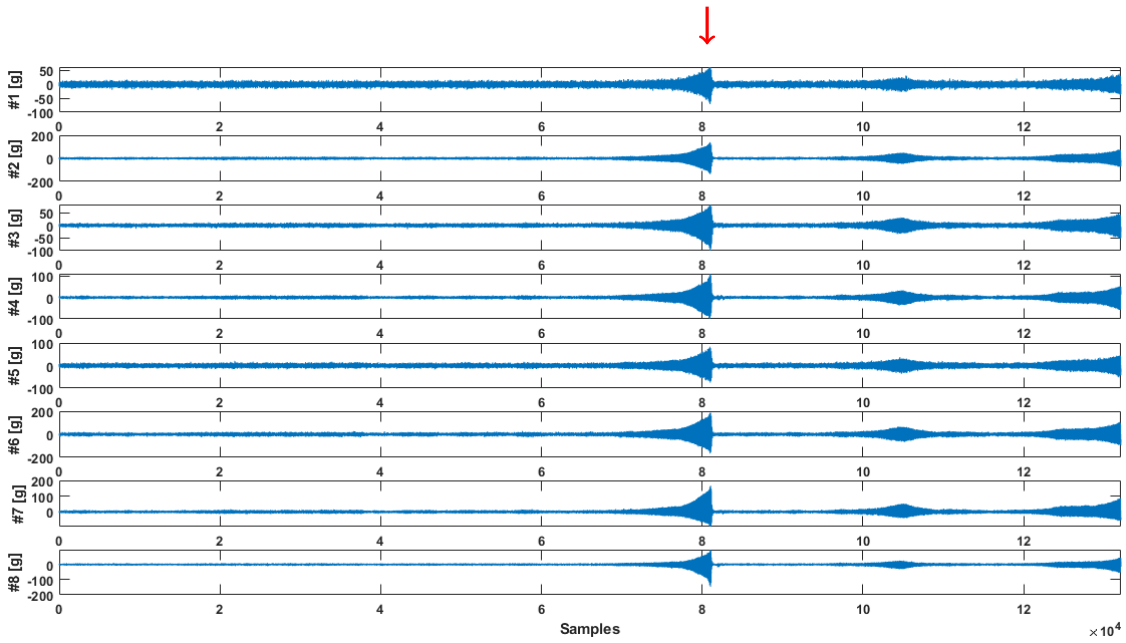

Figure 12: Flutter onset at angle of attack 3 degrees. Time signals from 8 accelerometers. The x-axis shows the time samples acquired with a sampling frequency of 2048 Hz. The red arrow marks the point at which the oscillations ceased due to the model being manually grasped.

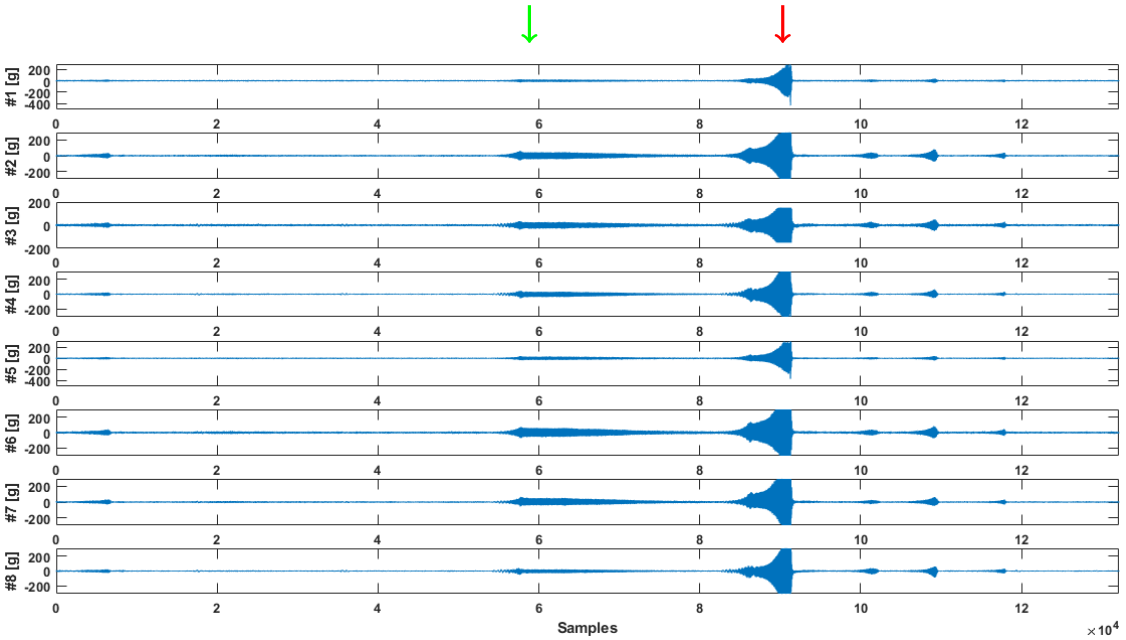

Figure 13: Flutter onset at angle of attack 5 degrees. Time signals from 8 accelerometers. The x-axis shows the time samples acquired with a sampling frequency of 2048 Hz. The green arrow marks the introduction of perturbations. The red arrow marks the point at which the oscillations ceased due to the model being manually grasped.

perturbation is sufficiently large to drive the system into rapidly increasing oscillations which must be interrupted with an external intervention to avoid damages.

LCO at angle of attack of 7 degrees (signal 2). The time response shown in Figure 15 is obtained with a dynamic pressure chosen in correspondence to the flutter onset and at a slightly higher dynamic pressure than the one shown in Figure 14 (548 Pa instead of 538 Pa). The wind tunnel turbulence is not sufficient to trigger the flutter onset at this specific dynamic pres-

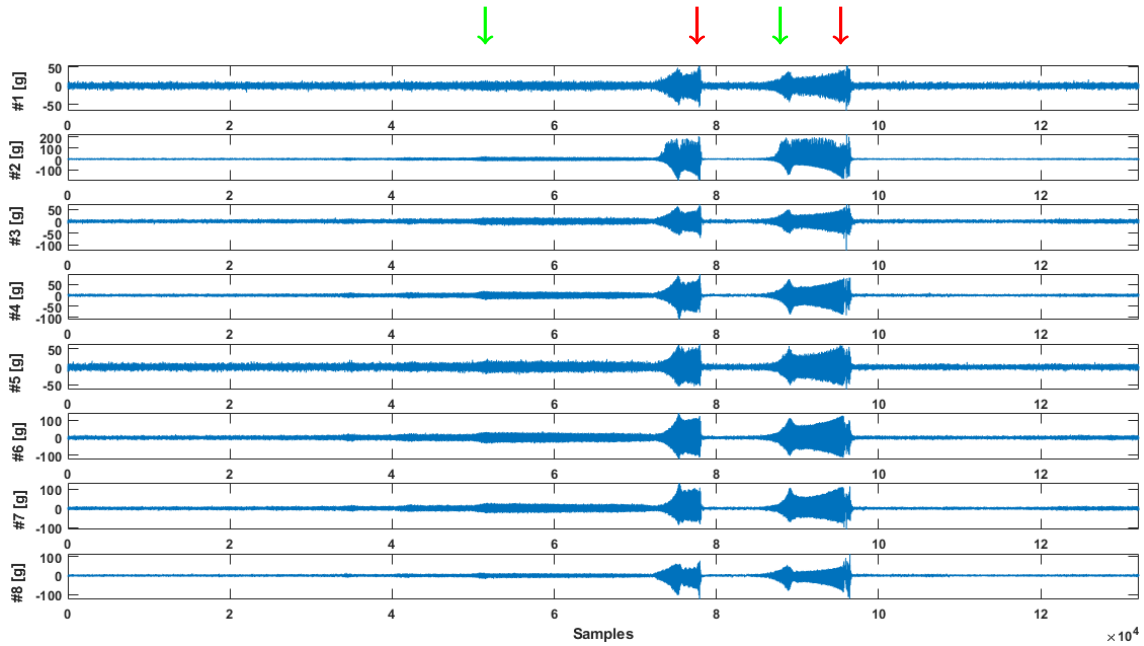

Figure 14: Flutter onset at angle of attack 7 degrees. Time signals from 8 accelerometers. The x-axis shows the time samples acquired with a sampling frequency of 2048 Hz. The green arrows mark the introduction of perturbations. The red arrows mark the point at which the oscillations ceased due to the model being manually grasped.

sure. Small perturbations are introduced in correspondence with the green arrows. The first one is not sufficient to move the system away from the trivial solution: the unstable LCO appears temporarily and subsequently subsides. The second perturbation is sufficiently large to drive the system into rapidly increasing oscillations which must be interrupted with an external intervention to avoid damages.

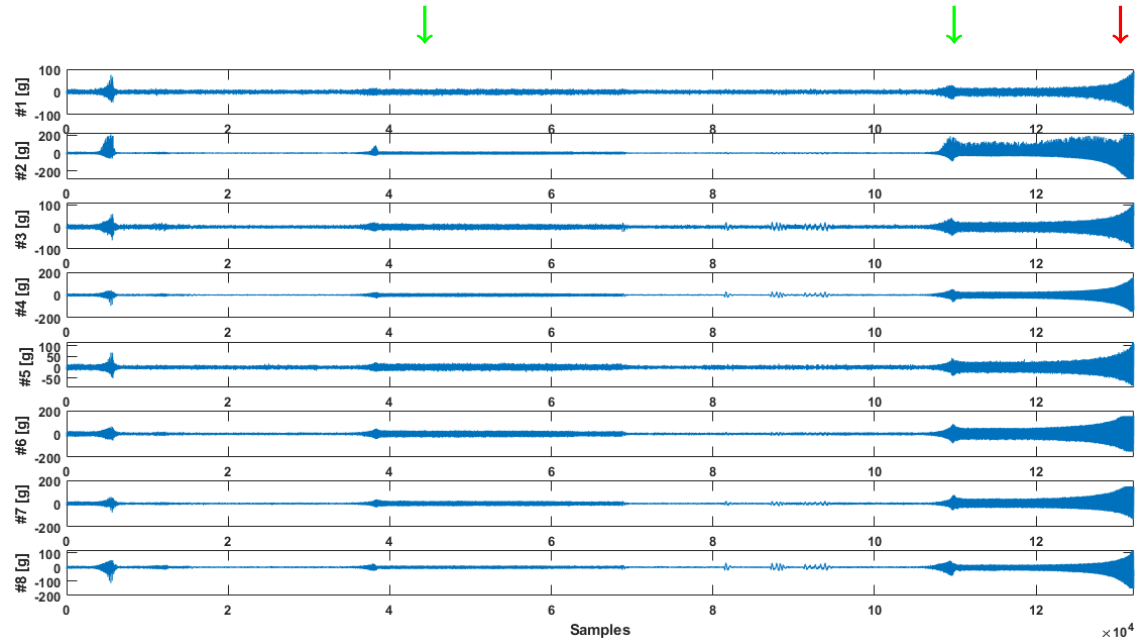

Figure 15: Flutter onset at angle of attack 7 degrees. Time signals from 8 accelerometers. The x-axis shows the time samples acquired with a sampling frequency of 2048 Hz. The green arrows mark the introduction of perturbations. The red arrow marks the point at which the oscillations ceased due to the model being manually grasped.

3.2 Experiments carried out in the Sapienza wind tunnel

Ahead of the measurements in the ZHAW wind tunnel, the same model was installed and tested in the Sapienza wind tunnel. A comparable flutter mechanism but a substantially different LCO were observed.

Due to the different test sections, the angle of attack in the open test section of the wind tunnel at Sapienza is equivalent in terms of static deflection to an angle six to seven degrees smaller in the closed test section of the ZHAW wind tunnel. A qualitative comparison is presented in Figure 16, in which the wing tip displacements predicted by the analytical model and four experimental points are plotted against the angle of attack. In previous experiments [26, 33] a good agreement between the predicted and measured static displacements was observed. Such a large difference is not surprising because (i) wind tunnel models installed inside a closed test section, with little clearance in our case, tend to affect the pressure distributions on wind tunnel walls in such a way that the effective angle of attack is greater then the geometric one, (ii) the effective angle of attack of wind tunnel models installed in open test sections tends to be smaller than the geometric one. Refer for instance to [46].

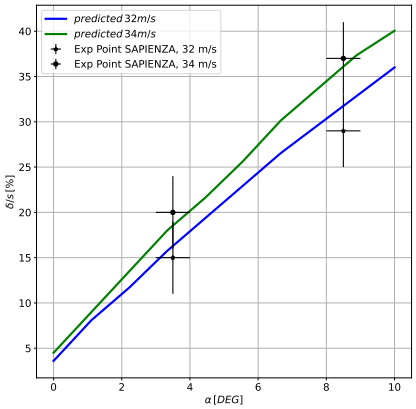

Figure 16: Static wing tip displacements predicted by the analytical model and measured in the Sapienza wind tunnel at root angle of attacks of 10 and 15 degrees. Qualitatively, a difference of six to seven degrees is observed.

3.2.1 Linear stability analysis

The root loci at 10 and 15 degrees root angle of attack are presented in Figure 17. The coalescence of the second bending and first torsional modes at wind speed close to 34 m/s is evident. The wind tunnel maximum speed was not sufficient to observe a complete flutter offset.

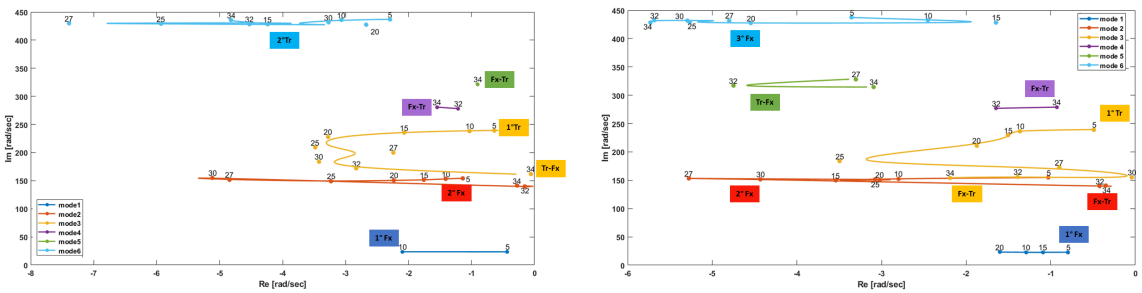

Figure 17: Root locus from the data measured in the Sapienza wind tunnel, at a root angle of attack of 10 (lhs) and 15 (rhs) degrees.

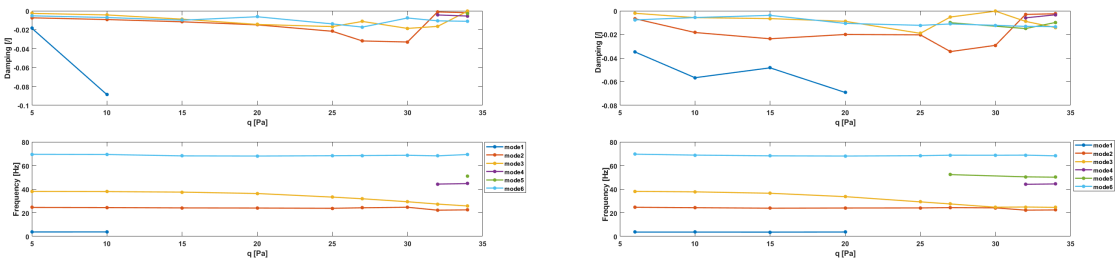

Figure 18: V-g plot from the data measured in the Sapienza wind tunnel, at a root angle of attack of 10 (lhs) and 15 (rhs) degrees.

3.2.2 LCO analysis

The LCO amplitude is plotted in Figure 19 against wind speed for different angles of attack. The oscillation seemed to increase progressively with speed except for the measurements at 15 degrees, where the amplitude was noticeably higher for one speed value. Despite the similar flutter mechanism, the LCO seems to be affected by a much stronger nonlinearity than those observed with the same model in the ZHAW wind tunnel and other experiments such as the one reported in Ref. [12].

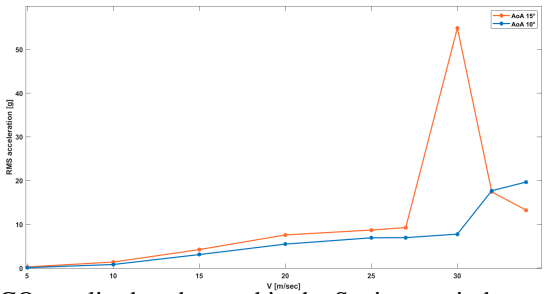

Figure 19: LCO amplitudes observed in the Sapienza wind tunnel campaign.

4 CONCLUSION

This study provided valuable insight into the dynamic response of very flexible wind tunnel models.

The specific model-to-wind tunnel attachment and the type of test section have a profound impact on the dynamic response. This is not surprising but the magnitude of these effects are worth mentioning. Similarly, manufacturing details can also affect the system's damping and the appearance of flutter and LCO.

The flutter mechanism observed in the wind tunnel aligns well with the predictions provided by a low-order analytical model, as confirmed by the results presented at the Third Aeroelastic Prediction Workshop [31]. This is merely a confirmation, based on a slightly different model.

The observed LCO are broadly consistent with the literature; however, our observations highlight the significant role of structural damping. Additionally, we clearly observed the typical onset associated with a subcritical LCO branch as we could unequivocally identify two and three distinct solutions appearing depending on the strnength of the excitation.

The experimental OMA methodologies used for the estimate of the modal parameters and the analytical model, considered for the reduction of the aeroelastic characteristics, proved both convenient and suitable to this specific problem.

To further enhance our understanding of this particular dynamic system, several actions can be taken. These include more precise tuning of the analytical model to the specific wind tunnel conditions and attempting to reproduce the LCO through time integration. Efforts to achieve this have been ongoing over the past few months, but have unfortunately been hindered by a series of numerical issues.

The authors are willing to share the experimental data with any interested parties.

5 REFERENCES

[1] Heeg, J. (2011). Aeroelastic Prediction Workshop 1 Website. `https://c3.ndc.nasa.gov/dashlink/static/media/other/AEPW_legacy.htm`. [Online; accessed 30.05.2024].

[2] Heeg, J. (2016). Aeroelastic Prediction Workshop 2 Website. `https://nescacademy.nasa.gov/workshops/AePW2/public/`. [Online; accessed 30.05.2024].

[3] Chwalowski, P. (2016). Aeroelastic Prediction Workshop 3 Website. `https://nescacademy.nasa.gov/workshops/AePW3/public/`. [Online; accessed 20.05.2024].

[4] Heeg, J., Ballmann, J., Bhatia, K., et al. (2011). Plans for an aeroelastic prediction workshop.

[5] Heeg, J., Chwalowski, P., Schuster, D. M., et al. (2015). Plans and example results for the 2nd AIAA Aeroelastic Prediction Workshop. *AIAA Paper*.

[6] Chwalowski, P., Heeg, J., and Biedron, R. T. (2017). Numerical investigation of the benchmark supercritical wing in transonic flow. In *58th AIAA/ASCE/AHS/ASC Structures, Structural Dynamics, and Materials Conference, AIAA SciTech Forum. American Institute of Aeronautics and Astronautics*, AIAA–2017–0190. doi:10.2514/6.2017-0190.

[7] Chwalowski, P., Massey, S. J., Jacobson, K., et al. (2022). Progress on transonic flutter and shock buffet computations in support of the third aeroelastic prediction workshop. In *AIAA Scitech 2022 Forum*. p. 1347.

[8] Heeg, J. (2013). Overview of the aeroelastic prediction workshop. In *51st AIAA aerospace sciences meeting including the new horizons forum and aerospace exposition*. p. 783.

[9] Heeg, J., Chwalowski, P., Raveh, D. E., et al. (2016). Overview and data comparisons from the 2nd aeroelastic prediction workshop. In *34th AIAA Applied Aerodynamics Conference*. p. 3121.

[10] Heeg, J. (2014). Unsteady aerodynamic validation experiences from the aeroelastic prediction workshop. In *52nd Aerospace Sciences Meeting*. p. 0203.

[11] Chwalowski, P. and Heeg, J. (2013). Fun3d analyses in support of the first aeroelastic prediction workshop. In *51st AIAA Aerospace Sciences Meeting including the New Horizons Forum and Aerospace Exposition*. p. 785.

[12] Drachinsky, A. and Raveh, D. E. (2020). Modal rotations: A modal-based method for large structural deformations of slender bodies. *AIAA Journal*, 58(7), 3159–3173.

[13] Avin, O., Raveh, D. E., Drachinsky, A., et al. (2022). Experimental aeroelastic benchmark of a very flexible wing. *AIAA Journal*, 60(3), 1745–1768.

[14] Goizueta, N., Drachinsky, A., Wynn, A., et al. (2021). Flutter predictions for very flexible wing wind tunnel test. In *AIAA Scitech 2021 Forum*. p. 1711.

[15] Ritter, M., Hilger, J., and Zimmer, M. (2021). Static and dynamic simulations of the pazy wing aeroelastic benchmark by nonlinear potential aerodynamics and detailed fe model. In *AIAA Scitech 2021 Forum*. p. 1713.

[16] Artola, M., Goizueta, N., Wynn, A., et al. (2021). Aeroelastic control and estimation with a minimal nonlinear modal description. *AIAA Journal*, 59(7), 2697–2713.

[17] Riso, C. and Cesnik, C. E. (2021). Correlations between um/nast nonlinear aeroelastic simulations and the pre-pazy wing experiment. In *AIAA Scitech 2021 Forum*. p. 1712.

[18] Avin, O., Raveh, D. E., Drachinsky, A., et al. (2021). An experimental benchmark of a very flexiblewing. In *AIAA Scitech 2021 Forum*. p. 1709.

[19] Righi, M. (2021). Uncertainties quantification in flutter prediction of a wind tunnel model exhibiting large displacements. In *AIAA Scitech 2021 Forum*. p. 1037.

[20] Riso, C. and Cesnik, C. (2022). Post-flutter dynamics of the pazy wing geometrically nonlinear benchmark model. In *International Forum on Aeroelasticity and Structural Dynamics (IFASD 2022)*.

[21] Righi, M. (2022). Uncertainties quantification in the flutter prediction of the pazy wing. In *International Forum on Aeroelasticity and Structural Dynamics (IFASD 2022)*.

[22] Mertens, C. (2022). Integrated aeroelastic measurements of the periodic gust response of a highly flexible wing. In *International Forum on Aeroelasticity and Structural Dynamics (IFASD 2022)*.

[23] Fehrs, M. (2022). Cfd simulations of the pazy wing in support of the third aeroelastic prediction workshop. In *International Forum on Aeroelasticity and Structural Dynamics (IFASD 2022)*.

[24] Riso, C. and Cesnik, C. (2022). Impact of low-order modeling on aeroelastic solution accuracy for very flexible wings. *Journal of Aircraft, accepted*.

[25] Riso, C. and Cesnik, C. E. S. (2023). Impact of low-order modeling on aeroelastic predictions for very flexible wings. *Journal of Aircraft*. doi:https://doi.org/10.2514/1.C036869.

[26] Righi, M. (2023). Uncertainties quantification in the prediction of the aeroelastic response of the pazy wing tunnel model. In *AIAA SCITECH 2023 Forum*. p. 0761.

[27] Pancini dos Santos, L. G., Cesnik, C. E., and Marques, F. D. (2024). Effects of separated-flow nonlinearities on the flutter behavior of the pazy wing. In *AIAA SCITECH 2024 Forum*. p. 0829.

[28] Lima, J. F., Luiz Bussamra, F., Verri, A. A., et al. (2024). Methodology to evaluate flutter on geometric nonlinear structural wings applied to the pazy wing. In *AIAA SCITECH 2024 Forum*. p. 0830.

[29] Righi, M., Coppotelli, G., Immordino, G., et al. *Experimental Characterization of Flutter and LCO of a Very Flexible Wing*. doi:10.2514/6.2024-0831.

[30] Riso, C. and Cesnik, C. E. (2022). Low-order geometrically nonlinear aeroelastic modeling and analysis of the pazy wing experiment. In *AIAA SCITECH 2022 Forum*. p. 2313.

[31] Ritter, M., Hilger, J., Ribeiro, A., et al. *Collaborative Pazy Wing Analyses for the Third Aeroelastic Prediction Workshop*. doi:10.2514/6.2024-0419.

[32] Righi, M., Greco, P., and Da Ronch, A. (2021). Uncertainties quantification of cfd-based flutter prediction. In *AIAA Scitech 2021 Forum*. p. 1038.

[33] Righi, M., Carnevali, L., and Ravasi, M. (2022). Uncertainties quantification in flutter prediction of a wind tunnel model exhibiting large displacements. In *AIAA SCITECH 2022 Forum*. p. 0178.

[34] Brincker, R., Zhang, L., and Andersen, P. (2000). Modal identification from ambient responses using frequency domain decomposition. In *XVIII IMAC, S. Antonio, TX, (USA), Society for Experimental Mechanics, Inc., Bethel, CT, USA*. pp. 625–630.

[35] Agneni, A., Crema, L. B., and Coppotelli, G. (2010). Output-only analysis of structures with closely spaced modes. *Mechanical System and Signal Processing. Special Issue: Operational Modal Analysis*, 24(5), 1240 – 1249.

[36] Overschee, P. V. and Moor, B. D. (1996). *Subspace Identification for Linear Systems*. Kluver Academic Publisher.

[37] Stanford, B. K., Jacobson, K. E., and Chwalowski, P. (2023). Aeroelastic analysis of highly flexible wings with linearized frequency-domain aerodynamics. *Journal of Aircraft*, 1–10.

[38] Ameri, N., Grappasonni, C., Coppotelli, G., et al. (2013). round vibration tests of a helicopter structure using oma techniques. *Mechanical Systems and Signal Processing*, 35(102), 35–51.

[39] Brincker, R. and Ventura, C. (2015). *Introduction to operational modal analysis*. John Wiley & Sons.

[40] Leishman, J. and Nguyen, K. (1990). State-space representation of unsteady airfoil behavior. *AIAA journal*, 28(5), 836–844.

[41] Berci, M. (2021). On aerodynamic models for flutter analysis: A systematic overview and comparative assessment. *Applied Mechanics*, 2(3).

[42] Theodorsen, T. (1949). General theory of aerodynamic instability and the mechanism of flutter. Tech. Rep. TR-496, NACA.

[43] Menter, F. R., Langtry, R. B., Likki, S., et al. (2006). A correlation-based transition model using local variables—part i: model formulation.

[44] Economon, T. D., Palacios, F., Copeland, S. R., et al. (2015). Su2: An open-source suite for multiphysics simulation and design. *AIAA Journal*, 54(3), 828–846. doi:10.2514/1.J053813.

[45] Dowell, E. H. (2014). *A modern course in aeroelasticity*, vol. 217. Springer.

[46] Barlow, J. B., Rae, W. H., and Pope, A. (1999). *Low-speed wind tunnel testing*. John wiley & sons.

COPYRIGHT STATEMENT